European Journal of Pharmaceutics and Biopharmaceutics 145 (2019) 65–75

Contents lists available at ScienceDirect

European Journal of Pharmaceutics and Biopharmaceutics

journal homepage: www.elsevier.com/locate/ejpb

Co-encapsulation of superparamagnetic nanoparticles and doxorubicin in PLGA nanocarriers: Development, characterization and *in vitro* antitumor efficacy in glioma cells

Edurne Luque-Michel[a,b], Víctor Sebastian[c,d,e,*], Ane Larrea[d], Clara Marquina[c,f], María J. Blanco-Prieto[a,b,*]

[a] Department of Pharmacy and Pharmaceutical Technology, School of Pharmacy, University of Navarra, C/Irunlarrea 1, E-31008 Pamplona, Spain
[b] Instituto de Investigación Sanitaria de Navarra (IdiSNA), Pamplona, Spain
[c] Instituto de Ciencia de Materiales de Aragón (ICMA), CSIC-Universidad de Zaragoza, C/Pedro Cerbuna 12, 50009 Zaragoza, Spain
[d] Institute of Nanoscience of Aragon (INA) and Department of Chemical, Engineering and Environmental Technology, University of Zaragoza, C/Mariano Esquillor, s/n, I+D+I Building, 50018 Zaragoza, Spain
[e] CIBER de Bioingeniería, Biomateriales y Nanomedicina (CIBER-BBN), Centro de Investigación Biomédica en Red, C/ Monforte de Lemos 3-5, Pabellón 11, 28029 Madrid, Spain
[f] Departamento de Física de la Materia Condensada, Universidad de Zaragoza, C/Pedro Cerbuna 12, 50009 Zaragoza, Spain

ARTICLE INFO

Keywords:
SPION
Tween 80
Pluronic F68
Brij- 35
Vitamin E-TPGS
PVA
Neurospheres
U87-MG
9L/LacZ

ABSTRACT

With a very poor prognosis and no clear etiology, glioma is the most aggressive cancer in the brain. Thanks to its versatility, nanomedicine is a promising option to overcome the limitations on chemotherapy imposed by the blood brain barrier (BBB). The objective of this paper was to obtain monitored tumor-targeted therapeutic nanoparticles (NPs). To that end, theranostic surfactant-coated polymer poly-Lactic-co-Glycolic Acid (PLGA) nanoplatform encapsulating doxorubicin hydrochloride (DOX) and superparamagnetic iron oxide NPs (SPIONs) were developed. Different non-ionic surfactants known as BBB crossing enhancers (Tween 80, Brij-35, Pluronic F68 or Vitamin E-TPGS) were used to develop 4 types of theranostic nanoplatforms, which were characterized in terms of size and morphology by DLS, TEM and STEM-HAADF analyses. Moreover, the 3-month stability test, the therapeutic efficacy against different glioma cell lines (U87-MG, 9L/LacZ and patient derived-neuronal stem cells) and the Magnetic Resonance Imaging (MRI) relaxivity were studied. Results showed that the synthesised nanoplatforms were stable at 4 °C after their lyophilization, being that of paramount importance to ensure a long-term stability in a future *in vivo* application. Furthermore, the theranostic nanoplatforms were efficient in the *in vitro* treatment of glioma cells, proving to have imaging efficacy as MRI contrast agents. Our results show an efficient loading of drugs and good value of the relaxivity. Therefore, the efficient theranostic hybrid nanoplatform developed here could be used to perform MRI-guided delivery of hydrophobic drugs.

1. Introduction

Among the various types of cancer that can affect the CNS, the glioblastoma (GBM) is considered the most lethal in both children and adults, even when treatment is given [1,2]. Many diagnostic and therapeutic strategies, such as the use of immunotherapy and new drugs are currently the subject of clinical trials [3]. However, until now there has been no real improvement, and the glioma treatment protocol has not changed since 2005, when a significant benefit in survival was demonstrated. The improvement was rationalized because the initial surgery to remove as much malignant mass as possible was followed by simultaneous radio- and chemotherapy with the alkylating agent prodrug temozolomide (Temodal®) [4]; only the antiangiogenic drug bevacizumab (Avastin®) is nowadays used in recurrent GBM [5]. Nevertheless, the resulting improvement was still poor, with a survival increase from 12.2 to 14.6 months [4]. Various difficulties are associated with treatment failure, beginning with the diffuse infiltration of the tumor, which complicates its complete removal during surgery, and

* Corresponding authors at: Department of Chemistry and Pharmaceutical Technology, School of Pharmacy, Universidad de Navarra, C/Irunlarrea 1, 31008 Pamplona, Spain. (M.J. Blanco-Prieto). 3Instituto de Ciencia de Materiales de Aragón (ICMA), CSIC-Universidad de Zaragoza, C/Pedro Cerbuna 12, 50009-Zaragoza, Spain. (V. Sebastian).
E-mail addresses: victorse@unizar.es (V. Sebastian), mjblanco@unav.es (M.J. Blanco-Prieto).

https://doi.org/10.1016/j.ejpb.2019.10.004
Received 1 August 2019; Received in revised form 15 September 2019; Accepted 16 October 2019
Available online 16 October 2019
0939-6411/

followed by the presence of cells with stem cell-like properties. These cancer stem cells (CSCs) initiate and boost the tumor by generating an aberrant GBM cell population. Moreover, they are resistant to the therapy used after surgery. In this scenario, tumor recurrence seems inevitable [5]. The chemotherapy options are highly limited by the blood brain barrier (BBB) that protects the brain from foreign toxins. Indeed, although at primary tumor sites the rapid expansion of the malignant mass can generate a rapid neoangiogenesis, losing tight junctions and leading to a disrupted BBB known as a blood brain tumor barrier (BBTB) [5], drug access is still limited since the brain microenvironment continues to compromise these fenestrations. In fact, intact regions can be maintained, while the porous ones formed are heterogeneous and smaller than those detected in tumors located in other organs [6,7].

Nanomedicine is an alternative that is currently being widely investigated in the treatment of brain cancer in the quest for nanocarriers targeting the BBB/BBTB. Interestingly, the composition and surface properties of these carriers influence their diffusion through the brain and even overcome the size hurdle [8]. Controlled and continued release of the drug in the tumor area could thus increase the tumor drug concentration and avoid the usual side effects. For instance, it has been widely demonstrated that nanosystems formed with the assistance of surfactant Tween 80 (T80) increase the amount of drug that reaches the brain [9–11]. In the bloodstream the T80-nanosystems are covered with apolipoprotein A or B and then endocytosed by the low-density lipoprotein (LDL) receptors, which are highly expressed in the BBB/BBTB cells [12]. Moreover, once they are inside the cell the glycoprotein P responsible for returning foreign compounds to the blood is inhibited by this surfactant [13]. Similarly, other surfactants have demonstrated that they have the potential to increase the BBB passage by inhibiting the action of the glycoproteing P such as poloxomers (Pluronics) [14,15], Vitamin E- TPGS (Tocopheryl polyethylene glycol 1000 succinate) [16–18] or Brij [13,19]. In addition, due to the inter-individual heterogeneity of the disease, the investigation of its individualized management is nowadays taking on a leading role. In this area, nanotechnology is also playing an important part. The use of nanosystems that can be followed by imaging techniques at the same time as they treat the tumor could move medicine forward towards the desired personalized therapy. Because of this, much of the current research is focused on the combination of therapeutic and diagnostic agents in the same nanosystem, so-called nanotheragnosis [8]. In other words, a theranostic nanopartform incorporates both imaging and therapeutic agents into one single probe [20]. Superparamagnetic iron oxide nanoparticles (SPIONs) can be followed by magnetic resonance imaging (MRI), as in the clinical trial of the MRI contrast imaging agent Ferumoxytol, which was designed to improve the viewing of tumors in patients with high-grade brain tumors or cancers that have spread to the brain [21]. These magnetic NPs modify the signal in the surrounding tissues, increasing the sensitivity of the technique, and making possible to monitor them. Therefore, loading magnetic NPs together with a GBM therapeutic agent can be a way to track the GBM therapy. Moreover, thanks to the magnetic properties of these NPs, they can also be used as hyperthermia or magnetic-targeting agents [22,23].

In this paper we explain how we developed and characterized theranostic hybrid polymeric NPs (HPNPs) formulated by the simple emulsion and solvent evaporation method. Poly-Lactic-co-Glycolic Acid (PLGA) was selected as polymer due to its well-known properties in terms of biocompatibility and biodegradability. In addition, PLGA enables the drug protection from biochemical degradation and the sustained release of encapsulated drugs [24]. Our hypothesis is that the encapsulation of the SPION and the cytostatic drug doxorubicin hydrochloride (DOX) jointly in the polymeric NP (PNP) would permit the fine-tuning of the GBM treatment, with MRI-guided delivery, and adaptation to the patient's response.

2. Material and methods

2.1. SPION-DOX HPNPs synthesis

DOX was purchased from Sigma and SPIONs were synthesized by the thermal decomposition of iron (III) acetylacetonate in the presence of polyol at a high temperature [25]. Briefly, 200 mg of iron (III) acetylacetonate ([Fe(acac)$_3$] (≥97%) purchased from Sigma-Aldrich) and 30 mL of triethylene glycol (99%, purchased from Sigma-Aldrich) were mixed in a three-neck flask and heated at a heating rate of 15 °C/min, up to 180 °C. The reaction was kept at this temperature for 30 min to induce decomposition of the [Fe(acac)$_3$] precursor. Afterwards, the three-neck flash was heated at a heating rate of 5 °C/min to reach the boiling temperature of the solvent (558 K). The reacting mixture was kept under reflux for 30 min and then cooled to room temperature. After reaction, a black colloid was obtained and the SPIONs were washed with a mixture of ethyl acetate and ethanol and separated using a magnet. The washing cycle was repeated at least 3 times.

Both DOX and SPIONs were encapsulated in PNPs to obtain HPNPs. First of all, different PLGAs (Resomer® 502, 503, 752 with free carboxylic or ester end groups) and organic solvents (ethyl acetate (EA), dichloromethane (DM) or acetone), as well as the amount of surfactant (1 or 2%) were tuned to optimize DOX encapsulation. Besides, triethylamine (TEA) or oleic acid were studied in different proportions (1:10, 1:100 and 1:1000) to dissolve DOX in the organic phase. Once the DOX concentration was optimized, the SPION encapsulation was tuned. For that, the multiple (w/o/w) or the simple (o/w) emulsion and solvent evaporation methods and the surfactants T80, Brij-35, Pluronic F68 and Vitamin E-TPGS were studied. The HPNPs formulated without DOX or SPION were synthesized in the same way. Finally, magnetization measurements at 310 K were performed in a high- sensitivity Superconducting Quantum Interference Device (SQUID) magnetometer (Quantum Design MPMS-XL), being 4 T the maximum applied d.c. magnetic field.

To synthesize SPION-DOX HPNPs by the multiple (w/o/w) emulsion and solvent evaporation method, 1 mg of DOX was dissolved in 1 mL of TEA: EA (1:1000), overnight and under stirring. 50 mg of PLGA and 50 μL of an aqueous suspension of SPION (7445 Fe ppm) were added to the solution. The mixture was sonicated for 20 s at 20 Watts in an ice bath using a Microson Ultrasonic Cell Disruptor XL (Branson sonifier 450, Branson Ultrasonics corp., EEUU) and then poured into 2 mL of water with 1% (w/w) surfactant. The mixture was sonicated again under the same conditions and added to 10 mL of an aqueous solution containing 0.3% (w/w) surfactant. After 1.5 h of magnetic agitation at room temperature, the ethyl acetate was evaporated and the HPNPs were formed. Afterwards, HPNPs were purified and collected by centrifugation at 17,000 g for 10 min at 4 °C. The purification process was repeated 3 times.

When the simple (o/w) emulsion and solvent evaporation method was used to synthesize SPION-DOX HPNPs, the SPIONs were functionalized with oleic acid to improve their dispersion in apolar solvents such as EA. The SPIONs were incubated with oleic acid (10 mg of iron/mL of oleic acid) for 24 h under stirring. Afterwards, they were centrifuged twice at 17,000 g for 5 min at 4 °C and suspended in the same volume of absolute ethanol and DM. Then, 0.2 mL of SPIONs (7445 Fe ppm) were added to 0.8 mL of EA: TEA (1:1000) containing 1 mg of DOX and 50 mg of PLGA previously dissolved. The resulting suspension was added to 2 mL of an aqueous solution with 1% (w/w) surfactant. Finally, the mixture was sonicated for 20 s at 20 Watts in an ice bath before being added to 10 mL of an aqueous 0.3% (w/w) surfactant solution. The solvent evaporation and HPNP purification process was carried out as previously described for HPNPs produced by multiple (w/o/w) emulsion.

2.2. SPION-DOX HPNP characterization

The hydrodynamic size and surface charge of the HPNPs were characterized using a Zetasizer Nano ZS (Malvern Instruments, UK). Transmission electron microscopy (TEM) was used to study the size, morphology and SPION distribution inside the HPNPs. TEM images were recorded on a T20-FEI Tecnai thermoionic microscope operated at an acceleration voltage of 200 kV. Negative stained samples were prepared by dropping 20 μL of sample in carbon coated copper grids (200 mesh), dried at room temperature and stained with a negative staining agent (phosphotungstic acid). Aberration corrected scanning transmission electron microscopy (Cs-corrected STEM) images were acquired using a high angle annular dark field detector (HAADF) in a FEI XFEG TITAN electron microscope operated at 300 kV and equipped with a CETCOR Cs-probe corrector from CEOS. Elemental analysis was carried out with an EDS (EDAX) detector which allows EDS experiments to be performed in the scanning mode.

The DOX loading efficiency was determined by fluorimetry and UV/vis spectrophotometry. DOX fluorescence was measured in a Tecan GENios microplate reader (Tecan Group Ltd, Maennedorf, Switzerland) at an excitation and emission wavelength of 485 and 580 nm; DOX absorbance was measured at 485 nm in a microplate PowerWave XS Microplate Spectrophotometer (BioTek). The calibration curves consisted in serial dilutions of DOX in dimethyl sulfoxide (DMSO) with a matrix of NPs synthesized without the drug. The SPIONs encapsulation was studied by measuring the iron spectrum at 300 nm using an Agilent 4100 MP-AES (Microwave Plasma - Atomic Emission Spectrometry) system [26]. Additionally, the SPION's oleic acid functionalization was confirmed with a Fourier-Transform Infrared Spectroscopy (FTIR) analysis.

2.3. Optimization of the lyophilization process for long-term stability of SPION-DOX HPNP

HPNPs covered with the different surfactants were lyophilized for 2 days in a LyoAlfa 6–50 laboratory freeze dryer (230 V, 50 Hz; Telstar). The composition of the HPNPs was optimized in order to obtain a high quality reconstitution sample-powder after the lyophilization process. To this end, it was studied the influence of: (1) adding different amounts of three cryoprotectors (trehalose, glucose and mannitol), (2) the amount of surfactants in the external phase of the emulsion (1 or 2%) and (3) an extra addition of PVA (polyvinyl alcohol MW 85,000–124,000 Da, 97–99% hydrolyzed) (from 0 to 0.6%) in the last solvent evaporation step. In all cases, their influence on the size, the superficial charge and morphology after the reconstitution of the HPNPs was characterized. Moreover, the residual PVA in the formulations was measured following the protocol of Sanjeeb K. Sahoo et al. [27]. Briefly, lyophilized HPNPs (2 mg) were treated with NaOH (0.5 M, 2 mL) for 15 min at 60 °C. After the treatment, they were neutralized with HCl (1 N, 0.9 mL) and the volume was adjusted to 5 mL with distilled water. Later, boric acid (0.65 M, 3 mL), a solution of I_2/KI (0.05 M/0.15 M, 0.5 mL) and distilled water (1.5 mL) were added to each sample; and after 15 min of incubation the absorbance was measured at 690 nm (Agilent 8453 UV–Vis Spectroscopy System, Agilent Technologies, Waldbronn Germany). The calibration curve of PVA was prepared under identical conditions [28].

2.4. Stability study

Physical and chemical stability studies of lyophilized NPs were carried out over 3 months. A batch of HPNPs was lyophilized and divided to be stored under 3 different conditions: room temperature (RT), 4 °C and 40 °C. Then, the hydrodynamic size of the HPNPs and their DOX load were measured immediately after being lyophilized and 1, 3, 4, 8 and 12 weeks after lyophilization, by the respective techniques above described.

2.5. Relaxivity study

To verify the diagnostic capability of the HPNPs by MRI, the relaxivity for the SPION-DOX HPNPs was measured by Time Domain Nuclear Magnetic Resonance (NMR) in a ^{1}H NMR Bruker Minispec Mq60, applying a magnetic field of 1.5 Tesla at 37 °C. Both the longitudinal (T1) and transversal (T2) relaxation time were measured to obtain the longitudinal (r1) and transversal (r2) relaxivity. To measure T1 and T2 the sequences Inversion Recovery (IR) and Carr-Purcel-Meiboom-Gill were used. To check the reproducibility of the results, three measurements of each concentration were made on the same day as well as on subsequent days.

2.6. Cell studies

2.6.1. Cell cultures

From the American Type Culture Collection (ATCC), 9L/lacZ gliosarcoma rat cell line (ATCC® CRL-2200™) was cultured in DMEM, and human glioblastoma U-87 MG (ATCC® HTB-14™) cells were cultured in DMEM/F12. Both media were complemented with 1% (v/v) penicillin-streptomycin and 5% (v/v) Fetal Bovine Serum (FBS), all from Gibco. Human neurosphere stem cell line (NSC-23) obtained from a patient from the hospital *Clínica Universidad de Navarra* (Spain) was grown in DMEM-F12-Glutamax (Thermofisher) completed with 10% B27 supplement (Gibco), 1% (v/v) penicillin-streptomycin, FGF-2 (basic Fibroblast Growth Factor) at 20 ng/mL (Inmuno Tool) and EFG (epidermal growth factor) at 20 ng/mL (Sigma). Cells were cultured at 37 °C and 5% CO_2 and every 3–4 days when cells were approximately 80% confluent (80% of surface of flask covered by cell monolayer) or the spheres formed were quite large, 1:5 splits were performed.

2.6.2. Cytotoxic efficacy study

To quantify the cytotoxic effect of SPION-DOX HPNPs, the *in vitro* cell viability was assessed by the CellTiter 96® AQueous One Solution Cell Proliferation Assay (MTS) colorimetric method. This method measures the metabolic activity of the mitochondrial NADPH dehydrogenases by means of the MTS-tetrazolium salt reduction into a water soluble formazan product. Three cell lines were used: the glioma cell line 9L, the human glioma cell line U87 and a human neurosphere stem cell NSC-23 obtained from a patient at the *Clínica Universidad de Navarra* (Spain).

In the case of the adherent cell lines 9L and U87, 3×10^3 and 2×10^3 cells/well, respectively, were seeded on a sterile 96-plate. After 24 h of incubation (at 37 °C and 5% of CO_2) to allow cell adhesion, the medium was replaced with DOX, SPION, DOX HPNPs, SPION HPNPs or SPION-DOX HPNPs at increasing concentrations (from 0 to 50 μg/mL) of DOX or equivalent. 48 or 72 h after the treatments, the medium was replaced with a dilution of MTS (15 μL MTS/100 μL cellular medium) and 2 h later the intensity of the color due to the formazan produced was measured spectrophotometrically (at λ = 492 and 690 nm). For the NSC-23 cells, which are cultured in suspension, 8×10^3 cells/well were plated and treated the same day; the same protocol as that used for adherent cells was followed. At the end of the experiments, the concentration of DOX that killed 50% of the cells after a specified exposure time (i.e. the half maximal effective concentration, EC50) was calculated. In this way, the smaller the EC50 value, the more effective the treatment was. For EC50 calculation, the data were adjusted to a logarithmic curve by the GraphPad Prism Software; data were expressed as mean ± standard deviation (SD).

3. Results and discussion

3.1. SPIONs synthesis and characterization

Fig. 1A and 1B present representative TEM micrographs of the obtained SPIONs dispersed in water. The SPIONs were of roughly

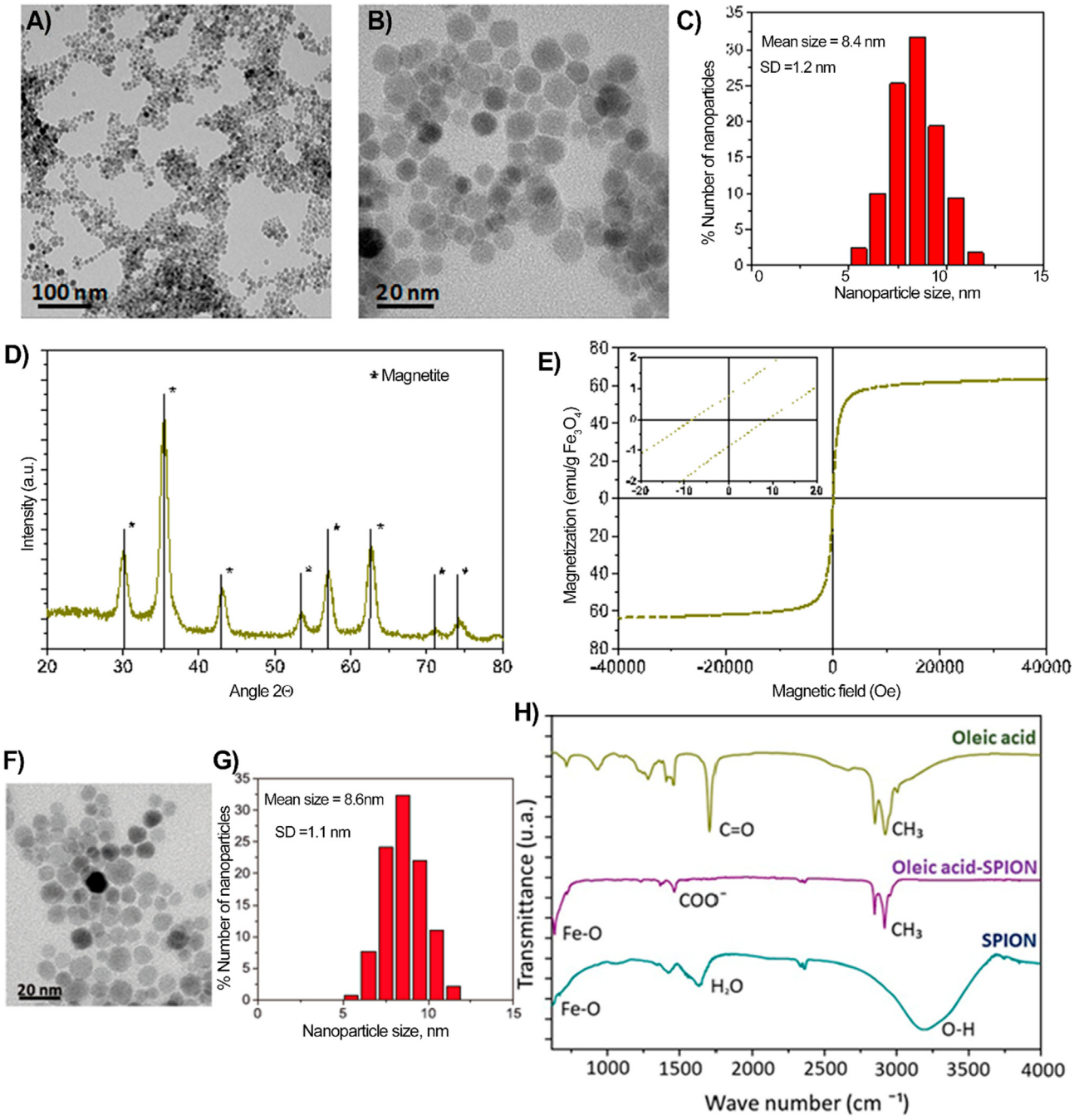

Fig. 1. Characterization of SPIONs. A) Low magnification TEM image, B) High magnification TEM image, C) Particle size histogram obtained from TEM images *measured using Image J software (sampling 200 NP)*, D) XRD pattern (reflections of magnetite, Fe_3O_4, are included for comparison), E) Magnetization curve at 310 K; inset: low field magnification. Characterization of oleic acid functionalized SPIONs. F) High magnification TEM image, G) Particle size histogram obtained from TEM images and h) FTIR spectrum of oleic acid, SPION (in water) and SPION functionalized with oleic acid (in dichloromethane).

spherical morphology, monodisperse in size, and apparently well dispersed. Fig. 1C depicts the particle size distribution histogram determined by statistical analysis of TEM images, resulting in an average particle size of 8.4 nm, with 1.2 nm standard deviation. The X-ray diffraction pattern of the SPIONs is shown in Fig. 1D. The XRD pattern was assigned to the bulk magnetite phase [Joint Committee on Powder Diffraction Standards (JCPDS) card number 89–0691]. The lattice parameter (a) of this material was calculated from the position of the (3 1 1) peak, resulting in a value of approximately 8.36 Å, which could be associated with magnetite (8.39 Å), magnetite (8.33–8.39 Å), or a solid mixture between the two phases [29]. Finally, the magnetic behavior of SPIONs at 310 K is shown in Fig. 1E. The NPs displayed superparamagnetic behavior, with a saturation magnetization of 64 emu/g. The coercive field seen in the low field magnification of the magnetization isotherm (see inset in Fig. 1E) corresponds to the residual offset field in the superconducting coil, after measuring at a field as high as 4 T. Therefore, this coercive field is only apparent and not a sign of hysteretic behavior [30].

SPIONs were functionalized with oleic acid in order to favor their dispersion in apolar solvents and then their loading in single o/w emulsions. Fig. 1F depicts a representative TEM image of oleic acid functionalized SPIONs, where no morphology differences were observed in comparison with the not functionalized SPIONs. The particle size distribution histogram (Fig. 1G) shows that the average particle

size was of 8.6 nm, with 1.1 nm standard deviation. The oleic acid coating of the SPION was confirmed by FTIR spectroscopy. Fig. 1H represents the FTIR spectra in the range of 600 to 4000 cm^{-1} of pure oleic acid, SPION in water and SPION functionalized with oleic acid (oleic acid-SPION) in DM. In the spectrum corresponding to the oleic acid-SPION, the peaks at 2924 and 2854 cm^{-1} denote the vibration of the functional CH_3 groups of the oleic acid, while the peak at 620 cm^{-1} corresponds to the vibration of the Fe-O bond of the SPION. However, the intense peak at 1710 cm^{-1} in the pure oleic spectrum corresponding to a C═O functional group (the responsible for the carboxylic linkage between oleic acid and SPION) is absent. Instead of this one the peak at 1464 cm^{-1}, characteristic of the asymmetric tension vibrations of the functional group COO−, is observed, what reveals that the oleic acid is adsorbed chemically on the SPION as a carboxylate. The peaks detected in the spectrum of the non-functionalized SPION in water are typically obtained in aqueous solutions [31,32].

3.2. SPION-DOX HPNPs synthesis optimization

SPION-DOX HPNPs were formed by the multiple or the simple emulsion and solvent evaporation method. First of all, the encapsulation of DOX and SPION in the PNP was optimized independently, and then the coencapsulation of both components was performed jointly. To optimize DOX encapsulation, different types of polymers based on PLGAs, organic solvents and the surfactant concentration were studied. To solubilize DOX in the organic phase, TEA or oleic acid were added to the organic phase in different proportions (see Table S1 in supplementary material). Interestingly, the encapsulation of DOX might be regarded as a consequence of its solubility in the different phases before the solidification of the polymer and NP formation. With respect to the PLGA polymer nomenclature, the first two numbers indicate the proportion of monomers (lactic acid and glycolic acid), and the final H indicates that the terminal group is an acid group instead of an ester. On the other hand, the third number that appears in the code, indicates the molecular weight [33,34]. As can be seen in Table S1, more DOX remains in the organic phase when PLGA 503H is used, showing a higher encapsulation in comparison with the other types of PLGAs. The PLGA 503H has a lactic acid: glycolic acid monomer proportion equal to 50:50 and an acid terminal group. Lactic acid is more hydrophobic than glycolic acid, and 503H is more hydrophobic than PLGA 752H (75:25), resulting in a higher encapsulation of the hydrophobic complex DOX-TEA/oleic acid. The PLGA 503H has a higher molecular weight than the 502H, yielding a high density of acid groups for which DOX has affinity [35]. With respect to the solvent used, EA has a higher elution power than DM and achieves the best encapsulation in comparison with the combination of DM with higher elution solvents (DM: EA (3:1) or DM: acetone (3:1)). Besides, the presence of more non-ionic surfactants in the aqueous phases could increase the solubility of the hydrophobic complex DOX-TEA/oleic acid in the aqueous phases decreasing its presence in the organic phase and its final encapsulation. Finally, as suggested in the literature [36–38], both TEA and oleic acid could be used to improve the solubility of DOX in organic solvents; in our case, just the addition of TEA resulted in a slight increase in the DOX solubility.

All in all, the highest DOX encapsulation efficacy was reached using the simple o/w emulsion method with PLGA 503H, EA: TEA (1:1000) and 1% of surfactant. Then, from that composition, the SPION encapsulation was independently tuned. As depicted in Fig. 2, the multiple w/o/w emulsion method was not effective to encapsulate the SPION properly, yielding a segregation of SPIONs and PLGA NPs (Fig. 2A and B), as well as a low SPION load. On the other hand, the simple o/w method, where the SPIONs were functionalized with oleic acid and dispersed in apolar solvents, rendered homogeneously distributed SPIONs inside the HPNPs (Fig. 2C). Differently from the multiple emulsification process, the simple emulsion enabled a selective loading of SPIONs in PLGA NPs. Importantly, the co-encapsulation of DOX and SPIONs did not influence the distribution of SPIONs inside the NPs (Fig. 2D), and HPNPs with a uniform size and spherical shape were obtained.

3.3. SPION-DOX HPNP characterization

Considering the importance of increasing the BBB passage by inhibiting the action of the glycoprotein P, we studied the production of SPION-DOX HPNPs using different types of surfactants (T80, Brij-35, Pluronic F68 and Vitamin E-TPGS). Table 1 shows a summary of the most relevant physico-chemical properties of the resulting HPNPs. A narrow size distribution of hydrodynamic diameters between 209 and 230 nm was found by DLS. The polydispersity index (PDI) less than 0.1 indicates that the sample consisted of a single size mode, without aggregates. The zeta-potential value (-13.8/-17.8 mv) ensures that the HPNPs will repel each other and avoid aggregation. The average diameter of the HPNPs obtained from TEM images (Fig. 3) is found to be well-correlated with that obtained from DLS measurements. The sizes determined by TEM are smaller than those obtained by DLS due to the lack of hydration during the electron microscopy analysis [39]. In addition, this difference could be also caused by the sensitivity of the DLS technique to particle agglomeration, to DOX fluorescence [40] or to “soft” flexible molecules such as polymers (like PVA), which could cause significant frictional drag influencing the particle motion [41,42]. With respect to DOX and SPION encapsulation, the results were similar for all HPNPs produced. The DOX load, measured fluorimetric- and spectrophotometrically, was around 10 μg DOX/ mg of HPNP (1% (w/w)), corresponding to a good encapsulation efficiency of 80%. The total SPION encapsulation was around 20 μg Fe/mg of NP (2% (w/w)). It is important to highlight that traditional physical methods of encapsulation in nanoplatforms, such as nanoprecipitation, lead to very poor encapsulation, due to the lack of sufficient carrier-cargo affinity and the limited void space in the nanoplatform to retain the cargo. The cargo loading is typically less than 5% (w/w) [43], or up to 18% in the case of Mosafer J. et al encapsulating SPIONs [44,45].

3.4. Optimization of the lyophilization process for long-term stability of SPION-DOX HPNP

Lyophilization was selected to improve the long-term stability of the HPNPs, preventing their instability in suspension and, simultaneously, facilitating their handling and storage. A good lyophilizate should maintain the physical and chemical properties of the original product, and the powder obtained should have a good appearance, a short reconstitution time, low residual moisture content and good long term conservation [46]. The SPION-DOX HPNPs freeze-dried without cryoprotectant changed their morphology and increased considerably in size after the lyophilized powder was reconstituted. The addition of cryoprotectors and different surfactant concentrations were tested although only the addition of the cryoprotector trehalose (37%; w/w with respect to the amount of PLGA) slightly enhanced the reconstitution. Interestingly, PVA had a major influence on the reconstitution when added in the last step of the NP synthesis. In fact, 0.4% PVA is the minimum amount for a good reconstitution. As can be seen in the size comparison before and after the lyophilization (Fig. 4A), the higher the PVA concentration, the better was the reconstitution. The NP morphology and the SPION distribution inside the HPNPs were maintained after lyophilization (Fig. 5). This PVA content represented around 5% of the total weight of the HPNP (Fig. 4B), less than in the case of other reported synthesis procedures that use PVA as a surfactant in the external phase of the emulsification process (13%) [27]. The block copolymer character of the partially hydrolyzed PVA could interact in the HPNP formation and explain the considerable improvement in HPNP stability during lyophilization [47]. In fact, the addition of PVA also affected the physicochemical properties of the HPNP, which increased in size and decreased their surface charge (Fig. 4C-D), indicating that

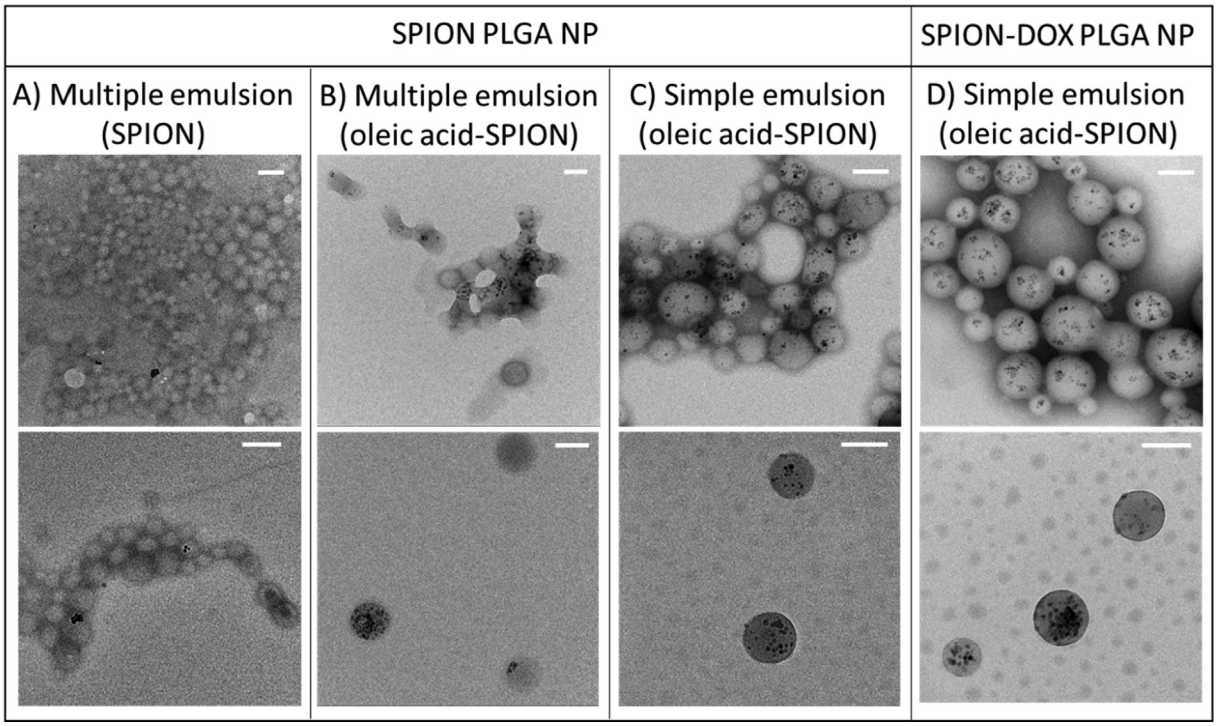

Fig. 2. TEM images of the NPs developed obtained by different synthesis methods: By multiple w/o/w emulsion method with A) SPIONs and with B) oleic acid functionalized SPIONs; and by simple o/w emulsion method with C) oleic acid functionalized SPIONs, and D) co-encapsulation of oleic acid-SPIONs and DOX. White scale bars represent 50 nm.

Table 1
Characterization of the SPION-DOX PLGA HPNPs. Hydrodynamic diameter, polydispersity index (PDI), Z potential and amount of DOX and Fe encapsulated.

Surfactant used	Hydrodynamic size (nm)	PDI	Z potential (mV)	DOX (μg/mg formulation)		Fe (μg/mg formulation)
				Fluorimetry	UV/vis spectroph.	
T80	227.4 ± 18.2	0.066 ± 0.021	−13.8 ± 3.3	11.2 ± 1.9	9.9 ± 1.4	17.8 ± 1.8
Brij-35	209.1 ± 26.5	0.077 ± 0.019	−16.8 ± 2.9	10.7 ± 0.8	10.2 ± 1.3	20.3 ± 1.5
Pluronic F68	211.9 ± 7.7	0.076 ± 0.017	−15.8 ± 2.1	10.7 ± 0.9	10.5 ± 1.0	17.7 ± 3.9
Vitamin E-TPGS	227.9 ± 55.8	0.107 ± 0.019	−17.8 ± 1.7	11.1 ± 2.8	10.8 ± 3.9	21.9 ± 3.6

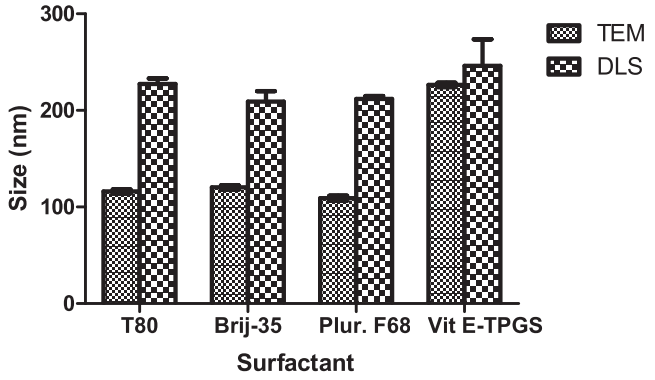

Fig. 3. Hydrodynamic diameter of the SPION-DOX PLGA NPs measured by DLS and diameter measured on TEM images *using Image J software* (around 150 NP).

the PVA was present on the surface of the NP. Certainly, the effect achieved could be compared to the effect of coating with hydrophilic polymers such as polyethylene glycol (PEG), resulting in a higher hydrophilicity [27]. A labile adsorption of PVA on the surface of the HPNP was appreciated when, in contrast to the findings by Murakami H. et al. [48], a decrease in PVA content was observed with the increased numbers of washings by centrifugation. Finally, Fig. 6 A- C depicts representative STEM-HAADF images at different magnifications of HPNPs lyophilized according to the optimized method and dispersed again in water. In this case, and unlike in TEM images, no staining agent was used to avoid artefacts that may occur during the staining process due to the presence of the cryoprotectant agents. The bright contrast of the STEM-HAADF images denotes the presence of high atomic number atoms, such as Fe. From this results, it can be ratified that SPIONs are located inside PLGA NPs, and that the lyophilization procedure preserves the structure and morphology of the HPNP. Fig. 6 D shows the energy-dispersive X-ray spectroscopy analysis (EDS) of the brightest NPs loaded in the PLGA NPs, in which the Fe signal confirms univocally the presence of SPIONs.

3.5. Stability study

To assess the stability, each type of HPNP was characterized in terms of size and amount of DOX after being formulated and lyophilized. Then, they were divided into 3 aliquots to be stored at 4, 25 (RT) or 40 °C. After an aging period of 1, 3, 4, 8 and 12 weeks, HPNPs were reconstituted in water and characterized. It should be mentioned that the copolymer PLGA has the possibility of modulating its rate of degradation by varying the molecular weight and the ratio of the monomers in the copolymer. As lactic acid is more hydrophobic than glycolic acid, PLGA enriched in lactic acid absorbs less water and consequently degrades more slowly [33,34]. In terms of size, the HPNPs stored at 4 °C

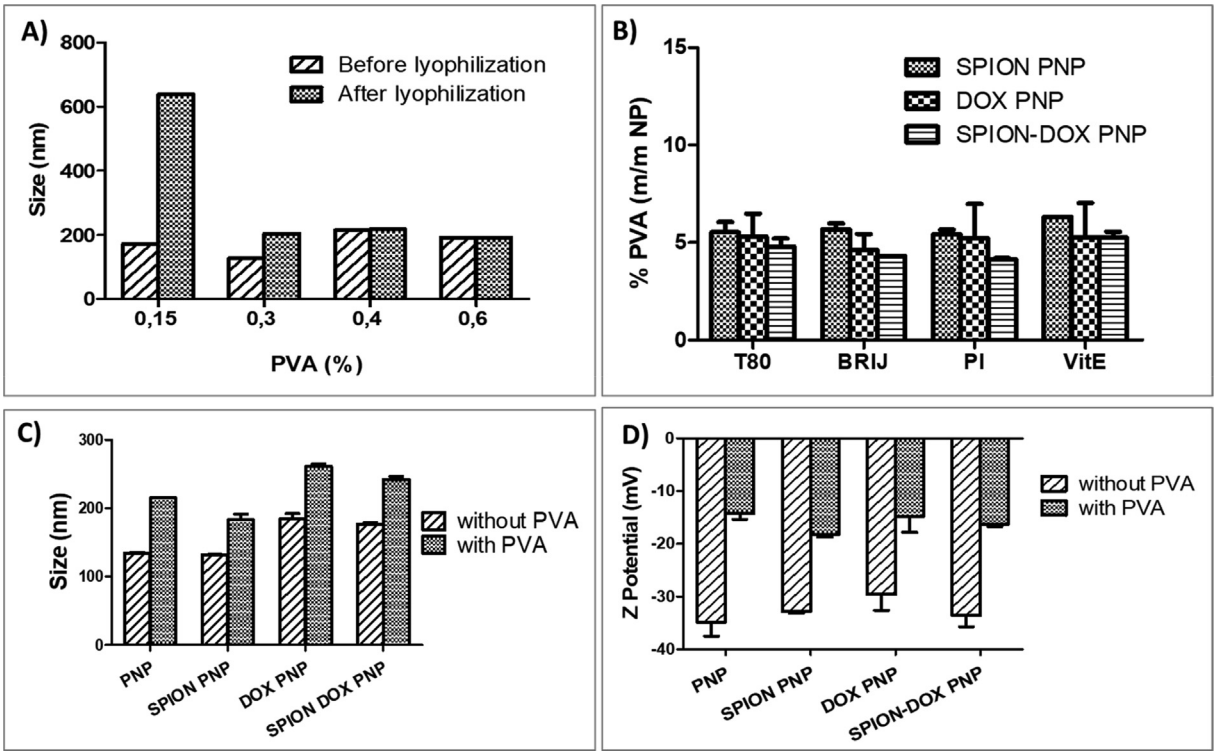

Fig. 4. Characterization of PVA addition to the formulation process of polymeric NP (PNP) with the surfactant T80. A) Hydrodynamic diameter before and after lyophilization, as a function of the amount of PVA, B) Residual percentage of PVA with respect to the weight of the HPNPs after their lyophilization. C) Influence of PVA addition on the hydrodynamic diameter. D) Influence of PVA addition on the surface charge.

remained stable throughout the study (Fig. 7A), those stored at RT were only stable during the first month; and those stored at 40 °C were not stable, since in 1 week their size increased considerably losing the homogeneity of the reconstituted HPNPs and being not possible to obtain a hydrodynamic size measurement by DLS (PDI = 1) (data not shown). With respect to the drug stability, the inherent fluorescence of DOX, associated with the central anthracycline chromophore group, has a strong dependence on the microenvironment and the formation of DOX dimers or DOX–iron complexes. Thus, as the degradation of the HPNPs was significant, it could also decrease the fluorescence intensity. In parallel, the drug loading in HPNPs was also determined by the optical absorbance of DOX, which is less sensitive and is not influenced by the microenvironment, dimerization or iron-complex formation [49–51]. Fig. 7B shows how the presence of DOX was maintained over time at all the storage temperatures when it was measured spectrophotometrically. But interestingly, when DOX was measured

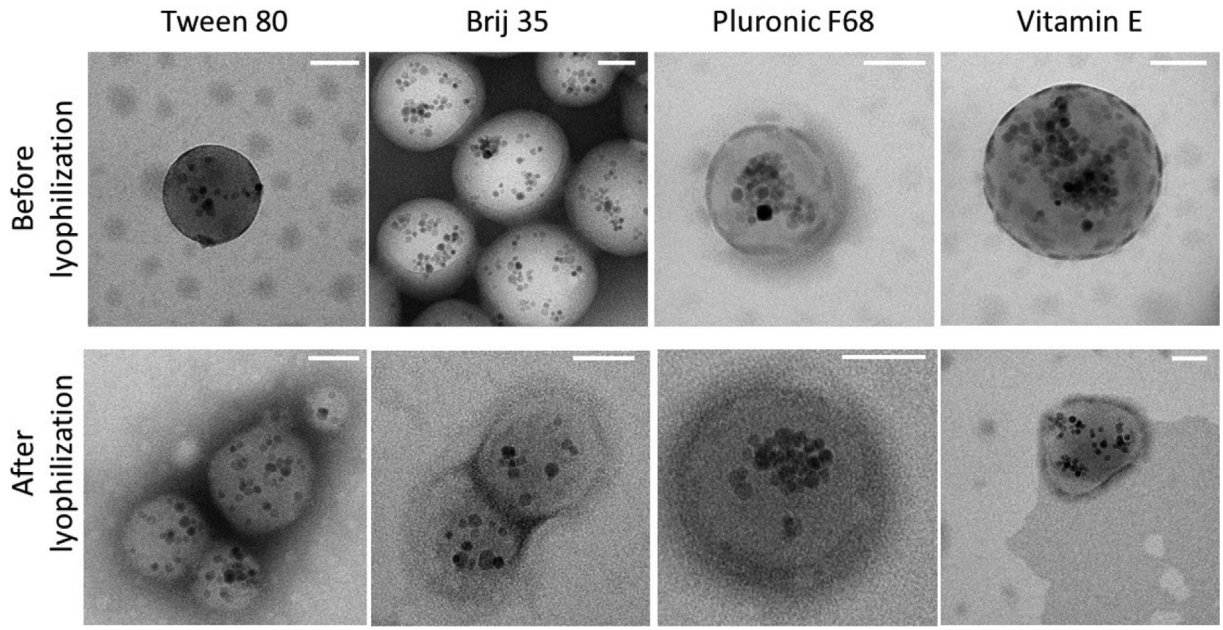

Fig. 5. TEM images of SPION-DOX HPNPs before and after their lyophilization and subsequent reconstitution. All NPs maintained their morphology and SPION distribution after lyophilization. White scale bars represent the size of 20 nm.

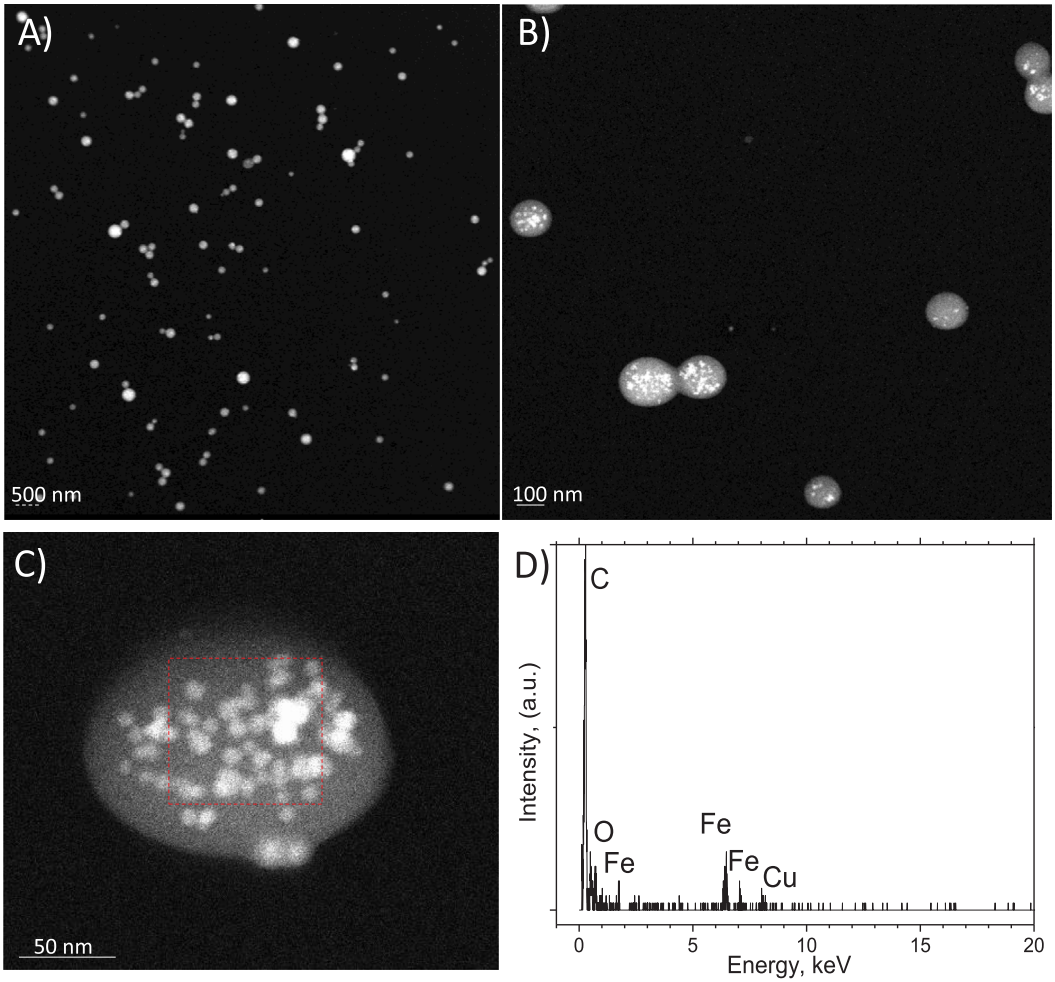

Fig. 6. A-C) Z-contrast STEM-HAADF images of representative HPNPs; bright spots show the location of SPIONs, D) HAADF-EDS analysis of the area selected in the HPNP in (C) to confirm the presence of SPIONs.

fluorimetrically (Fig. 7C), the drug load decreased considerably at RT and 40 °C and it was only stable at 4 °C throughout the experiment. This fact indicates that the structure of the HPNPs was preserved only at 4 °C for the 3 months of the experiment. Furthermore, considering that free DOX is a labile molecule which needs to be stored at –20 °C, the HPNPs developed greatly protect the drug from degradation.

3.6. Relaxivity study

Magnetic resonance signals have their origin in the Nuclear Magnetic Resonance of the hydrogen protons present in the medium, characterized by the longitudinal (T1) and transversal (T2) relaxation times. Contrast agents modify the NMR signal by increasing the relaxation velocities, i.e., the inverse of the T1 and T2, according to the so-called r1 and r2 relaxivities. The decrease of the relaxation times occurs in a concentration-dependent manner so that the relaxation velocity increases linearly with contrast agent concentration. The slope of these dependences is the relaxivity, a measure of how efficient the agent is for accelerating the longitudinal and transversal relaxation processes [52]. The relaxivity of the SPION-DOX HPNPs in aqueous suspension was obtained by measuring the relaxation times of the hydrogen protons of the water at different NP concentrations (from 0.1 to 1 mM [Fe^{+2}]). The results had good reproducibility and, as would be expected from a superparamagnetic nanoparticle system, r_2 was much larger than r_1 (Table 2). In detail, r_1 was 1.85, 0.28, 0.20 and 0.14 $mM^{-1}s^{-1}$; and r_2 was 197.80, 172.09, 158.03 and 160.15 $mM^{-1}s^{-1}$ for the NP synthesized with T80, Brij-35, Pluronic F68 or Vitamin E-TPGS, respectively. These r_2 values were very similar to those obtained using SPIONs already commercialized as contrast agents (Feridex r_2 = 120 $mM^{-1}s^{1}$; Resovist-Ferucarbotran r_2 = 189 $mM^{-1}s^{1}$) and indicate that these HPNPs could be used as contrast agents for magnetic susceptibility-based acquisitions in T2-weighted or T2*-weighted MRI, in which they would produce a hypointense (dark) signal [53].

3.7. Cytotoxic efficacy study

The cytotoxic efficacy of SPION-DOX HPNPs was examined in different glioma cell lines by the viability MTS assay. In the case of the commercial glioma cell lines U87 and 9L (Fig. 8 A and E), the EC50 after 48 h of treatment was around 20 μg/mL, for all the synthesized SPION-DOX HPNPs [54]. In more detail, the cytotoxic effect against 9L after 48 h was slightly smaller than that of the control (free DOX), matching approximately the same value at 72 h. This indicated a time-dependence cytotoxicity, probably due to still-conserved controlled drug release from the HPNP [55]. On the other hand, as in glioma tumors, neurospheres are a complex group of cells sustained by stem cells [56]. These stem cells are multipotent and have auto-regeneration capabilities; in GBM they are responsible for the initial formation and progression of the tumor, as well as for the treatment resistance and subsequent recurrence [57]. Therefore, the tumor-initiating cells that are resistant to current therapies should be targeted, and therapies that destroy cancer stem cells are potentially curative [58]. A picture of NSC-23 cells in culture is shown in Fig. 8B. These three dimensional

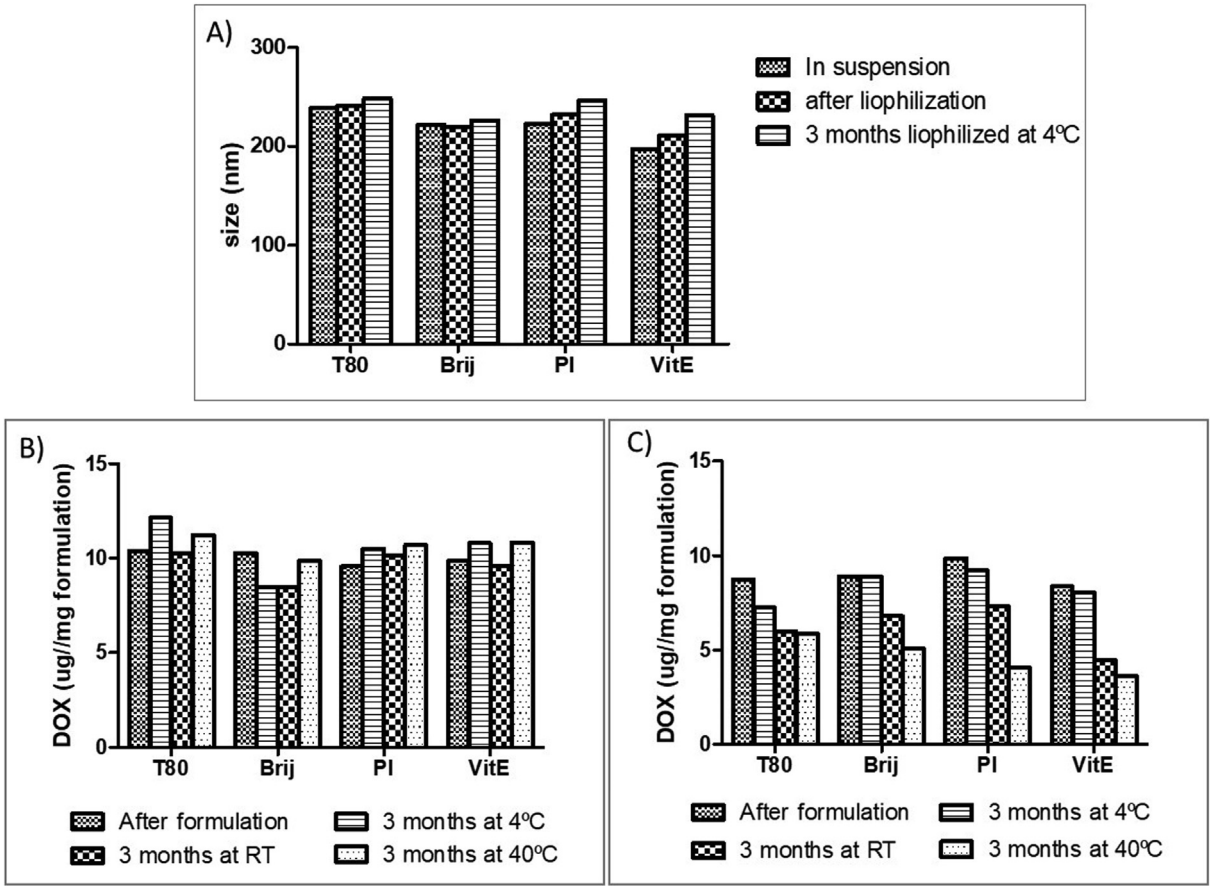

Fig. 7. Lyophilized HPNPs stability for 12 weeks. A) Hydrodynamic diameter before, immediately after and 12 weeks after being lyophilized and stored at 4 °C. B) Spectrophotometric and C) fluorimetric measurement of DOX load before and 12 weeks after being lyophilized and stored at RT, 4 or 40 °C.

Table 2
Longitudinal (r1) and transversal (r2) relaxivity of the SPION-DOX PLGA HPNPs.

Surfactant used	r1 ($mM^{-1}s^{-1}$)	r2 ($mM^{-1}s^{-1}$)
T80	1.85	197.80
Brij-35	0.28	172.09
Pluronic F68	0.20	158.03
Vitamin E-TPGS	0.14	160.15

(3D) culture models closely mimic the heterogeneity and the microenvironment of the *in vivo* conditions, and thus allow a more predictive *in vitro* evaluation of nanomedicines [59]. Similar EC50 was obtained for encapsulated and non-encapsulated DOX at 72 h of treatment (Fig. 8A).

For all of these 3 cultures, SPION-DOX HPNPs inhibited cell viability in a dose-dependent manner; the type of surfactant used to form the HPNPs did not influence the cytotoxic effect. Both control NPs, SPION and SPION-PLGA NP, were found to be non-toxic at the concentrations used (see the representative graphic in Fig. 8C and D), indicating that the drug alone was responsible for the observed toxicity. In conclusion, these *in vitro* results suggest that all SPION-DOX HPNP developed in this study are potent treatments and thus promising candidates for *in vivo* efficacy studies.

4. Conclusions

The surfactants Tween 80, Brij-35, Pluronic F68 and Vitamin E-TPGS were used to design and develop four different surfactant-coated HPNPs for the theranostic of glioma. These surfactants were selected to increase the passage of the HPNPs through the BBB after an intravenous injection. On the other hand, DOX and SPIONs were selected as therapeutic and imaging agents, respectively, in order to achieve real time monitoring of the treatment by MRI. The HPNPs developed have a high DOX and SPIONs encapsulations and only adding 0.4% of PVA in the last step of their synthesis was enough to achieve good stability of the lyophilized powder at 4 °C for 3 months, facilitating the management and storage of the HPNPs. Significantly, these HPNPs proved to be promising MRI-monitoring nanocarriers since they presented high transversal relaxivity as expected by superparamagnetic NPs. Besides, the nanocarriers provided therapeutic effects not only in normal population glioma cells but also in neuronal cells with stem cell properties, which are the principal cause of the resistance to conventional therapies in brain tumors.

Acknowledgements

Edurne Luque-Michel thanks the Government of Navarra for the dissertation research fellowship. Clara Marquina thanks the Spanish Ministry of Economy and Competitiveness for financial support from project MAT2016-78201-P. Authors would like to acknowledge the use of Servicio General de Apoyo a la Investigación-SAI, Universidad de Zaragoza.

Appendix A. Supplementary material

Supplementary data to this article can be found online at https://doi.org/10.1016/j.ejpb.2019.10.004.

A)

Cell line	T80		Brij-35		Pluronic F68		Vitamin E-TPGS		DOX
	S-D	D	S-D	D	S-D	D	S-D	D	
U87 48h	26.2	35.9	17.8	14.0	23.2	16.9	21.2	20.0	18.2
9L 48h	29.0	46.3	26.4	36.7	31.3	23.8	33.9	35.4	21.0
9L 72 h	77.1	NS	85.8	NS	68.1	NS	83.4	NS	74.1
NSC 23 72h	6.2	NS	15.3	NS	9.3	NS	12.3	NS	7.0

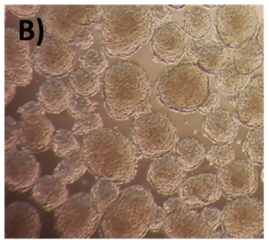

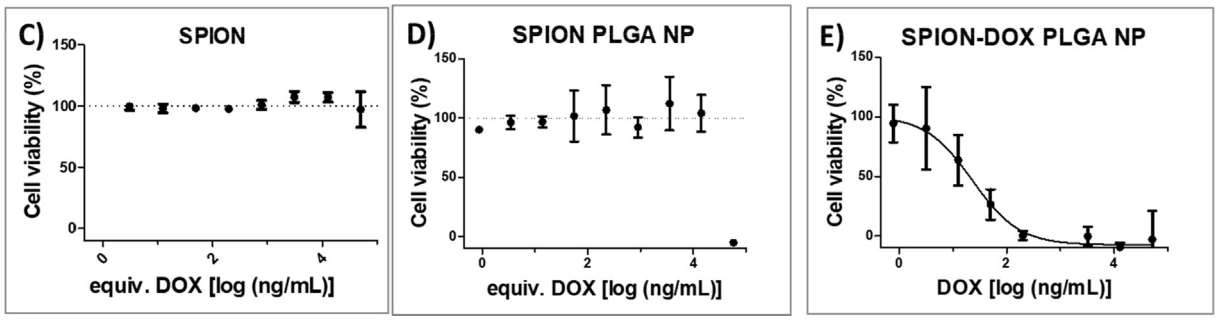

Fig. 8. A) EC50 (ng/mL) of SPION-DOX HPNPs, DOX PLGA NPs and DOX formulated with the surfactants T80, Brij-35, Pluronic F68 or Vitamin E-TPGS. EC50: half maximal effective concentration; NS = not studied; S-D = SPION-DOX HNPs; D = DOX PLGA NPs. B) Image of patient-donated neurospheres NSC-23. C, D, E) Representative graphics of cell viability vs DOX concentration in the treatment of U87-MG cells with SPION, SPION PLGA NPs or SPION-DOX HNPs.

References

[1] R. Azzarelli, B.D. Simons, A. Philpott, The developmental origin of brain tumours: a cellular and molecular framework, Development. 145 (2018) dev162693, https://doi.org/10.1242/dev.162693.

[2] J.T. Huse, E.C. Holland, Targeting brain cancer: advances in the molecular pathology of malignant glioma and medulloblastoma, Nat. Rev. Cancer. 10 (2010) 319–331, https://doi.org/10.1038/nrc2818.

[3] ClinicalTrials.gov, Search of: glioblastoma - List Results - ClinicalTrials.gov, (n.d.). https://clinicaltrials.gov/ct2/results?cond=glioblastoma&term=&cntry=&state=&city=&dist= (accessed June 27, 2018).

[4] R. Stupp, W.P. Mason, M.J. van den Bent, M. Weller, B. Fisher, M.J.B. Taphoorn, K. Belanger, A.A. Brandes, C. Marosi, U. Bogdahn, J. Curschmann, R.C. Janzer, S.K. Ludwin, T. Gorlia, A. Allgeier, D. Lacombe, J.G. Cairncross, E. Eisenhauer, R.O. Mirimanoff, Radiotherapy plus concomitant and adjuvant temozolomide for glioblastoma, N. Engl. J. Med. 352 (2005) 987–996, https://doi.org/10.1056/NEJMoa043330.

[5] L.P. Ganipineni, F. Danhier, V. Préat, Drug delivery challenges and future of chemotherapeutic nanomedicine for glioblastoma treatment, J. Control. Release. 281 (2018) 42–57, https://doi.org/10.1016/j.jconrel.2018.05.008.

[6] P.M. Peiris, A. Abramowski, J. Mcginnity, E. Doolittle, R. Toy, R. Gopalakrishnan, S. Shah, L. Bauer, K.B. Ghaghada, C. Hoimes, S.M. Brady-Kalnay, J.P. Basilion, M.A. Griswold, E. Karathanasis, Treatment of invasive brain tumors using a chain-like nanoparticle, Cancer Res. 75 (2015) 1356–1365, https://doi.org/10.1158/0008-5472.CAN-14-1540.

[7] S.K. Hobbs, W.L. Monsky, F. Yuan, W.G. Roberts, L. Griffith, V.P. Torchilin, R.K. Jain, Regulation of transport pathways in tumor vessels: role of tumor type and microenvironment, Proc. Natl. Acad. Sci. 95 (1998) 4607–4612, https://doi.org/10.1073/pnas.95.8.4607.

[8] E. Luque-Michel, E. Imbuluzqueta, V. Sebastián, M.J. Blanco-Prieto, Clinical advances of nanocarrier-based cancer therapy and diagnostics, Expert Opin. Drug Deliv. 14 (2017) 75–92, https://doi.org/10.1080/17425247.2016.1205585.

[9] A. Estella-Hermoso de Mendoza, V. Preat, F. Mollinedo, M.J. Blanco-Prieto, In vitro and in vivo efficacy of edelfosine-loaded lipid nanoparticles against glioma, J. Control. Release. 156 (2011) 421–426, https://doi.org/10.1016/j.jconrel.2011.07.030 [doi].

[10] D. Singh, H. Kapahi, M. Rashid, A. Prakash, A.B.A. Majeed, N. Mishra, Recent prospective of surface engineered Nanoparticles in the management of Neurodegenerative disorders, Artif. Cells, Nanomedicine Biotechnol. 44 (2016) 780–791, https://doi.org/10.3109/21691401.2015.1029622.

[11] B. Petri, A. Bootz, A. Khalansky, T. Hekmatara, R. Müller, R. Uhl, J. Kreuter, S. Gelperina, Chemotherapy of brain tumour using doxorubicin bound to surfactant-coated poly (butyl cyanoacrylate) nanoparticles: revisiting the role of surfactants, J. Control. Release. 117 (2007) 51–58, https://doi.org/10.1016/j.jconrel.2006.10.015.

[12] M. Gidwani, A.V. Singh, Nanoparticle enabled drug delivery across the blood brain barrier: in vivo and in vitro models, opportunities and challenges, Curr. Pharm. Biotechnol. 14 (2014) 1201–1212 (accessed July 2, 2018), http://www.ncbi.nlm.nih.gov/pubmed/24809717.

[13] F.G. Hoosain, Y.E. Choonara, L.K. Tomar, P. Kumar, C. Tyagi, L.C. du Toit, V. Pillay, Bypassing P-glycoprotein drug efflux mechanisms: possible applications in pharmacoresistant schizophrenia Therapy, Biomed Res. Int. 2015 (2015) 484963, https://doi.org/10.1155/2015/484963.

[14] S. Gelperina, O. Maksimenko, A. Khalansky, L. Vanchugova, E. Shipulo, K. Abbasova, R. Berdiev, S. Wohlfart, N. Chepurnova, J. Kreuter, Drug delivery to the brain using surfactant-coated poly(lactide-co-glycolide) nanoparticles: Influence of the formulation parameters, Eur. J. Pharm. Biopharm. 74 (2010) 157–163, https://doi.org/10.1016/j.ejpb.2009.09.003.

[15] T. Schuster, A. Mühlstein, C. Yaghootfam, O. Maksimenko, E. Shipulo, S. Gelperina, J. Kreuter, V. Gieselmann, U. Matzner, Potential of surfactant-coated nanoparticles to improve brain delivery of arylsulfatase A, 253 (2017) pp. 1–10. http://doi.org/10.1016/j.jconrel.2017.02.016.

[16] E.-M. Collnot, C. Baldes, M.F. Wempe, R. Kappl, J. Hüttermann, J.A. Hyatt, K.J. Edgar, U.F. Schaefer, C.-M. Lehr, Mechanism of inhibition of P-glycoprotein mediated efflux by vitamin E TPGS: influence on ATPase activity and membrane fluidity, Mol. Pharm. 4 (2007) 465–474, https://doi.org/10.1021/mp060121r.

[17] X. Meng, J. Liu, X. Yu, J. Li, X. Lu, T. Shen, Pluronic F127 and D-α-tocopheryl polyethylene glycol succinate (TPGS) mixed micelles for targeting drug delivery across the blood brain barrier, Sci. Rep. 7 (2017) 2964, https://doi.org/10.1038/s41598-017-03123-y.

[18] S.A. Kulkarni, S.-S. Feng, Effects of particle size and surface modification on cellular uptake and biodistribution of polymeric nanoparticles for drug delivery, Pharm. Res. 30 (2013) 2512–2522, https://doi.org/10.1007/s11095-012-0958-3.

[19] J.M. Koziara, P.R. Lockman, D.D. Allen, R.J. Mumper, In situ blood-brain barrier transport of nanoparticles, Pharm. Res. 20 (2003) 1772–1778 (accessed January 10, 2017), http://www.ncbi.nlm.nih.gov/pubmed/14661921.

[20] G. Jin, R. He, Q. Liu, M. Lin, Y. Dong, K. Li, B.Z. Tang, B. Liu, F. Xu, Near-infrared light-regulated cancer theranostic nanoplatform based on aggregation-induced emission luminogen encapsulated upconversion nanoparticles, Theranostics. 9 (2019) 246–264, https://doi.org/10.7150/thno.30174.

[21] O.K.C.I. Edward Neuwelt, Ferumoxytol in Improving MR Imaging in Patients With High-Grade Brain Tumors or Cerebral Metastases - Full Text View - ClinicalTrials.gov, (n.d.). https://clinicaltrials.gov/ct2/show/study/NCT00103038 (accessed September 11, 2018).

[22] J. Zhou, J. Zhang, W. Gao, Enhanced and selective delivery of enzyme therapy to 9L-glioma tumor via magnetic targeting of PEG-modified, β-glucosidase-conjugated iron oxide nanoparticles, Int. J. Nanomedicine. 9 (2014) 2905–2917, https://doi.org/10.2147/IJN.S59556.

[23] G. Yi, B. Gu, L. Chen, The safety and efficacy of magnetic nano-iron hyperthermia therapy on rat brain glioma, Tumor Biol. 35 (2014) 2445–2449, https://doi.org/10.1007/s13277-013-1324-8.

[24] V. Andreu, A. Larrea, P. Rodriguez-Fernandez, S. Alfaro, B. Gracia, A. Lucía, L. Usón, A.-C. Gomez, G. Mendoza, A. Lacoma, J. Dominguez, C. Prat, V. Sebastian, J.A. Ainsa, M. Arruebo, Matryoshka-type gastro-resistant microparticles for the oral treatment of *Mycobacterium tuberculosis*, Nanomedicine. 14 (2019) 707–726, https://doi.org/10.2217/nnm-2018-0258.

[25] N. Miguel-Sancho, O. Bomati-Miguel, A.G. Roca, G. Martinez, M. Arruebo, J. Santamaria, Synthesis of magnetic nanocrystals by thermal decomposition in glycol media: effect of process variables and mechanistic study, Ind. Eng. Chem. Res. 51 (2012) 8348–8357, https://doi.org/10.1021/ie3002974.

[26] R.P. Friedrich, C. Janko, M. Pöttler, P. Tripal, J. Zaloga, I. Cicha, S. Dürr, J. Nowak, S. Odenbach, I. Slabu, M. Liebl, L. Trahms, M. Stapf, I. Hilger, S. Lyer, C. Alexiou, Flow cytometry for intracellular SPION quantification: specificity and sensitivity in comparison with spectroscopic methods, Int. J. Nanomedicine. 10 (2015) 4185, https://doi.org/10.2147/IJN.S82714.

[27] S.K. Sahoo, J. Panyam, S. Prabha, V. Labhasetwar, Residual polyvinyl alcohol associated with poly (D, L-lactide-co-glycolide) nanoparticles affects their physical

properties and cellular uptake, J. Control. Release. 82 (2002) 105–114 (accessed July 5, 2018), http://www.ncbi.nlm.nih.gov/pubmed/12106981.
[28] T. Simón-yarza, F.R. Formiga, E. Tamayo, B. Pelacho, F. Prosper, M.J. Blanco-prieto, PEGylated-PLGA microparticles containing VEGF for long term drug delivery, Int. J. Pharm. 440 (2013) 13–18, https://doi.org/10.1016/j.ijpharm.2012.07.006.
[29] N. Miguel-Sancho, O. Bomatí-Miguel, G. Colom, J.-P. Salvador, M.-P. Marco, J. Santamaría, Development of stable, water-dispersible, and biofunctionalizable superparamagnetic iron oxide nanoparticles, Chem. Mater. 23 (2011) 2795–2802, https://doi.org/10.1021/cm1036452.
[30] M. Buchner, K. Höfler, B. Henne, V. Ney, A. Ney, Tutorial: Basic principles, limits of detection, and pitfalls of highly sensitive SQUID magnetometry for nanomagnetism and spintronics, J. Appl. Phys. 124 (2018) 161101, https://doi.org/10.1063/1.5045299.
[31] P. Velusamy, S. Chia-Hung, A. Shritama, G.V. Kumar, V. Jeyanthi, K. Pandian, Synthesis of oleic acid coated iron oxide nanoparticles and its role in anti-biofilm activity against clinical isolates of bacterial pathogens, J. Taiwan Inst. Chem. Eng. 59 (2016) 450–456, https://doi.org/10.1016/J.JTICE.2015.07.018.
[32] S. Masur, B. Zingsem, T. Marzi, R. Meckenstock, M. Farle, Characterization of the oleic acid/iron oxide nanoparticle interface by magnetic resonance, J. Magn. Magn. Mater. 415 (2016) 8–12, https://doi.org/10.1016/J.JMMM.2016.03.045.
[33] R.A. Jain, The manufacturing techniques of various drug loaded biodegradable poly (lactide-co-glycolide) (PLGA) devices, Biomaterials. 21 (2000) 2475–2490 (accessed September 14, 2018), http://www.ncbi.nlm.nih.gov/pubmed/11055295.
[34] A.A. Ignatius, L.E. Claes, In vitro biocompatibility of bioresorbable polymers: poly (L, DL-lactide) and poly(L-lactide-co-glycolide), Biomaterials. 17 (1996) 831–839 (accessed September 14, 2018), http://www.ncbi.nlm.nih.gov/pubmed/8730968.
[35] National Center for Biotechnology Information. PubChem Database., No Title, Doxorrubicin, CID = 31703. (n.d.). https://pubchem.ncbi.nlm.nih.gov/compound/31703 (accessed May 6, 2019).
[36] D. Missirlis, R. Kawamura, N. Tirelli, J.A. Hubbell, Doxorubicin encapsulation and diffusional release from stable, polymeric, hydrogel nanoparticles, Eur. J. Pharm. Sci. 29 (2006) 120–129, https://doi.org/10.1016/j.ejps.2006.06.003.
[37] Y.-C. Ma, J.-X. Wang, W. Tao, H.-S. Qian, X.-Z. Yang, Polyphosphoester-based nanoparticles with viscous flow core enhanced therapeutic efficacy by improved intracellular drug release, ACS Appl. Mater. Interfaces. 6 (2014) 16174–16181, https://doi.org/10.1021/am5042466.
[38] X. Zhang, X. Sun, J. Li, X. Zhang, T. Gong, Z. Zhang, Lipid nanoemulsions loaded with doxorubicin-oleic acid ionic complex: characterization, in vitro and in vivo studies, Pharmazie. 66 (2011) 496–505 (accessed May 4, 2019), http://www.ncbi.nlm.nih.gov/pubmed/21812324.
[39] E. Luque-Michel, A. Larrea, C. Lahuerta, V. Sebastian, E. Imbuluzqueta, M. Arruebo, M.J. Blanco-Prieto, J. Santamaria, A simple approach to obtain hybrid Au-loaded polymeric nanoparticles with a tunable metal load, Nanoscale. 8 (2016) 6495–6506, https://doi.org/10.1039/c5nr06850a [doi].
[40] J. Bteich, M.J. Ernsting, M. Mohammed, T. Kiyota, T.D. McKee, M. Trikha, H.B. Lowman, K.K. Sokoll, Nanoparticle formulation derived from carboxymethyl cellulose, polyethylene glycol, and cabazitaxel for chemotherapy delivery to the brain, Bioconjug. Chem. 29 (2018) 2009–2020, https://doi.org/10.1021/acs.bioconjchem.8b00220.
[41] W.-L. Lin, P.-C. Liang, Y.-C. Chen, C.-F. Chiang, L.-R. Mo, S.-Y. Wei, W.-Y. Hsieh, Doxorubicin-modified magnetic nanoparticles as a drug delivery system for magnetic resonance imaging-monitoring magnet-enhancing tumor chemotherapy, Int. J. Nanomedicine. 11 (2016) 2021, https://doi.org/10.2147/IJN.S94139.
[42] M.A. Dobrovolskaia, A.K. Patri, J. Zheng, J.D. Clogston, N. Ayub, P. Aggarwal, B.W. Neun, J.B. Hall, S.E. McNeil, Interaction of colloidal gold nanoparticles with human blood: effects on particle size and analysis of plasma protein binding profiles, nanomedicine nanotechnology, Biol. Med. 5 (2009) 106–117, https://doi.org/10.1016/j.nano.2008.08.001.
[43] K. Park, Facing the truth about nanotechnology in drug delivery, ACS Nano. 7 (2013) 7442–7447, https://doi.org/10.1021/nn404501g.
[44] J. Mosafer, M. Teymouri, Comparative study of superparamagnetic iron oxide/doxorubicin co-loaded poly (lactic-co-glycolic acid) nanospheres prepared by different emulsion solvent evaporation methods, Artif. Cells, Nanomedicine Biotechnol. 46 (2018) 1146–1155, https://doi.org/10.1080/21691401.2017.1362415.
[45] J. Mosafer, M. Teymouri, K. Abnous, M. Tafaghodi, M. Ramezani, Study and evaluation of nucleolin-targeted delivery of magnetic PLGA-PEG nanospheres loaded with doxorubicin to C6 glioma cells compared with low nucleolin-expressing L929 cells, Mater. Sci. Eng. C. 72 (2017) 123–133, https://doi.org/10.1016/j.msec.2016.11.053.
[46] P. Fonte, S. Reis, B. Sarmento, Facts and evidences on the lyophilization of polymeric nanoparticles for drug delivery, J. Control. Release. 225 (2016) 75–86, https://doi.org/10.1016/J.JCONREL.2016.01.034.
[47] M. Yang, S.K. Lai, T. Yu, Y.-Y. Wang, C. Happe, W. Zhong, M. Zhang, A. Anonuevo, C. Fridley, A. Hung, J. Fu, J. Hanes, Nanoparticle penetration of human cervicovaginal mucus: the effect of polyvinyl alcohol, J. Control. Release. 192 (2014) 202–208, https://doi.org/10.1016/j.jconrel.2014.07.045.
[48] H. Murakami, M. Kobayashi, H. Takeuchi, Y. Kawashima, Preparation of poly(dl-lactide-co-glycolide) nanoparticles by modified spontaneous emulsification solvent diffusion method, Int. J. Pharm. 187 (1999) 143–152, https://doi.org/10.1016/S0378-5173(99)00187-8.
[49] E. Munnier, S. Cohen-Jonathan, C. Linassier, L. Douziech-Eyrolles, H. Marchais, M. Soucé, K. Hervé, P. Dubois, I. Chourpa, Novel method of doxorubicin-SPION reversible association for magnetic drug targeting, Int. J. Pharm. 363 (2008) 170–176, https://doi.org/10.1016/j.ijpharm.2008.07.006.
[50] P. Mohan, N. Rapoport, Doxorubicin as a molecular nanotheranostic agent: effect of doxorubicin encapsulation in micelles or nanoemulsions on the ultrasound-mediated intracellular delivery and nuclear trafficking, Mol. Pharm. 7 (2010) 1959–1973, https://doi.org/10.1021/mp100269f.
[51] P. Changenet-Barret, T. Gustavsson, D. Markovitsi, I. Manet, S. Monti, Unravelling molecular mechanisms in the fluorescence spectra of doxorubicin in aqueous solution by femtosecond fluorescence spectroscopy, Phys. Chem. Chem. Phys. 15 (2013) 2937–2944, https://doi.org/10.1039/c2cp44056c.
[52] S. Laurent, L. Vander Elst, A. Roch, R.N. Muller, Structure, synthesis and characterization of contrast agents for magnetic resonance molecular imaging, NMR-MRI, MSR Mössbauer Spectrosc. Mol. Magnets, Springer Milan, Milano, 2007, pp. 71–87, , https://doi.org/10.1007/978-88-470-0532-7_3.
[53] J.S. Weinstein, C.G. Varallyay, E. Dosa, S. Gahramanov, B. Hamilton, W.D. Rooney, L.L. Muldoon, E.A. Neuwelt, Superparamagnetic iron oxide nanoparticles: diagnostic magnetic resonance imaging and potential therapeutic applications in neurooncology and central nervous system inflammatory pathologies, a review, J. Cereb. Blood Flow Metab. 30 (2010) 15–35, https://doi.org/10.1038/jcbfm.2009.192.
[54] L. Battaglia, M. Gallarate, E. Peira, D. Chirio, E. Muntoni, E. Biasibetti, M.T. Capucchio, A. Valazza, P.P. Panciani, M. Lanotte, D. Schiffer, L. Annovazzi, V. Caldera, M. Mellai, C. Riganti, Solid lipid nanoparticles for potential doxorubicin delivery in glioblastoma treatment: preliminary in vitro studies, J. Pharm. Sci. 103 (2014) 2157–2165, https://doi.org/10.1002/jps.24002.
[55] Y. González-Fernández, H.K. Brown, A. Patiño-García, D. Heymann, M.J. Blanco-Prieto, Oral administration of edelfosine encapsulated lipid nanoparticles causes regression of lung metastases in pre-clinical models of osteosarcoma, Cancer Lett. 430 (2018) 193–200, https://doi.org/10.1016/j.canlet.2018.05.030.
[56] E.V. Valenciano, D. De Fisiología, E. De Medicina, D. Universidad, D.C. Rica, C. Costarricense, D.S. Social, S. Jose, C. Rica, M. Ángel, E. Miranda, E. De Medicina, D. Universidad, D.C. Rica, C. Costarricense, D.S. Social, S. Jose, C. Rica, Importancia de Células madre tumorales y cultivos de neuroesferas en neurooncología, Neuroeje. 25 (2012) 55–60.
[57] R.P.M. Alicia, M. Mihaliak, Candace A. Gilbert, Li Li, Marie-Claire Daou, A.H.R. Andrew Reeves, Brent H. Cochranc, Clinically relevant doses of chemotherapy agents reversibly block formation of glioblastoma neurospheres, Cancer Lett. 296 (2010) 168–177, https://doi.org/10.1016/j.canlet.2010.04.005.
[58] M.M. Alonso, H. Jiang, C. Gomez-Manzano, J. Fueyo, Targeting brain tumor stem cells with oncolytic adenoviruses, Methods Mol. Biol. (2012) 111–125, https://doi.org/10.1007/978-1-61779-340-0_9.
[59] G. Lazzari, P. Couvreur, S. Mura, Multicellular tumor spheroids: a relevant 3D model for the: In vitro preclinical investigation of polymer nanomedicines, Polym. Chem. 8 (2017) 4947–4969, https://doi.org/10.1039/c7py00559h.